RSC Advances

ROYAL SOCIETY OF CHEMISTRY

www.rsc.org/advances

Graphical Abstract

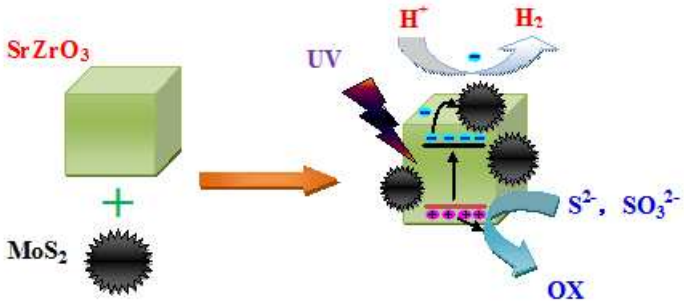

Cite this: DOI: 10.1039/c0xx00000x

www.rsc.org/xxxxxx

ARTICLE TYPE

Synthesis of $MoS_2/SrZrO_3$ heterostructures and their photocatalytic H_2 evolution under UV irradiation

Qingwen Tian,† Li Zhang,† Jiahui Liu, Naixu Li, Quanhong Ma, Jiancheng Zhou,* Yueming Sun

Received (in XXX, XXX) Xth XXXXXXXXX 20XX, Accepted Xth XXXXXXXXX 20XX
DOI: 10.1039/b000000x

A novel heterojunction of $MoS_2/SrZrO_3$ photocatalyst was successfully synthesized via simple hydrothermal process and applied to the photocatalytic H_2 evolution under UV light irradiation. The samples were characterized by X-ray diffraction, UV-vis absorption spectroscopy, scanning and transmission electron microscopy, X-ray photoemission spectroscopy, energy dispersive X-ray spectroscopy and EDX mapping. The heterostructure with an optimal content of 0.05 wt % MoS_2 exhibits the highest H_2 evolution rate of 5.31 mmol/h. This is due to the junction between $SrZrO_3$ and MoS_2, which suppresses the recombination of photogenerated electron and hole. Our work indicated that the prepared $MoS_2/SrZrO_3$ heterostructured photocatalyst can be used as an effective material for water splitting.

1. Introduction

Photocatalytic water splitting has attracted considerable attention due to the depletion of fossils and energy crisis challenging science[1-3], and hydrogen has been considered as one of the clean, economical and environmentally friendly energies in modern society[4-6]. Since the first report by Fujishima and Honda on electrochemical photolysis of water at TiO_2 electrode[7], great efforts have been made to explore hydrogen evolution to solve energy and enviromental issues[4, 8]. Selecting novel photocatalysts possessing wide range of light response and higher quantum efficiency, such as, heterogeneous photocatalysts, metal coordination photocatalysts [9], hierarchically structured nanocrystals [10,11] and et al, have been intensively and extensively investigated because of special band structure and the carrier transportation[12, 13].

Photocatalysts containing d^0 and d^{10} metal irons, such as,Ti^{4+}, Zr^{4+}, Nb^{5+}, Ga^{3+} and $Sb5^+$ have been demonstrated as higher photocatalytic activities for H_2 evolution under UV irradiation[4, 14]. Among them, perovskite type oxide ABO_3, where A is an alkaline metal or an alkaline earth metal and B is a transition metal [15], such as, $SrZrO_3$, $BaZrO_3$, $SrTiO_3$, $BiVO_4$ and etc, have been considered as one of the most promising photocatalysts due to its unique properties as high stability and nontoxicity[16]. Furthermore, perovskite-type $SrZrO_3$, with a wide band gap of 5.6 eV, has attracted much attention owing to its applications in high-temperature materials[17], luminescence properties[18], hydrogen gas sensors[19] and catalysts[20]. And excellent stabilities and more photocatalytic active sites make $SrZrO_3$ a suitable photocatalyst applied to the water splitting and dye degradation reactions under UV light irradiation.

Heterogeneous photocatalysis is considered as one of the most promising methods solving energy and environmental crisis, and perovskite type oxide compounds have been selected as one of the suitable materials[4, 14, 21]. On the other hands, layer-structured transition metal sulfide especially for MoS_2, which is consist of metal Mo attached with two S and stacking together to furnish sandwich-like structure, is also exploited for photocatalytic applications owing to its narrow band gap and high thermal stability[22, 23], and a great number of heterogeneous photocatalysts containing MoS_2 have been synthesized during the past decades [22, 24-28]. Li et al synthesized MoS_2/CdS catalyst and investigated the photocatalytic activities before and after loading MoS_2 under visible light irradiation, founding a greatly enhancement of H_2 evolution after loading MoS_2[29]. Liu et al prepared a novel photocatalyst with 3D hierarchical heterostructure, MoS_2/TiO_2, exhibiting an excellent photocatalytic H_2 evolution and dye degradation, impling the matched energy band of MoS_2/TiO_2 heterostructure favoring the charge transfer and suppression the recombination of photogenerated electron and hole between MoS_2 and TiO_2[27].

Herein, a novel heterostructured $MoS_2/SrZrO_3$ photocatalyst was synthesized by facile hydrothermal method. Then the as-prepared sample was employed to investigated photocatalytic H_2 evolution from aqueous solutions containing Na_2S and Na_2SO_3 under UV irradiation, and 0.05 wt % MoS_2 loading on the $SrZrO_3$ crystal was found to show best performance with H_2 evolution rate of 5.31 mmol/h. MoS_2 was proved to be an effective separation of

photogenerated carriers in the $MoS_2/SrZrO_3$ heterojunction and the possible mechanism of H_2 evolution was discussed. To the best of our knowledge, this is the first report onthe preparation of $MoS_2/SrZrO_3$ heterojunction and their application in the photocatalytic activity for water splitting under UV light irradiation.

2. Experimental Section

2.1 Chemicals and materials

Zirconium (Ⅳ) oxychloride octahydrate ($ZrOCl_2·8H_2O$), strontium nitrate ($Sr(NO_3)_2$), potassium hydroxide (KOH), sodium molybdate dehydrate ($Na_2MoO_4·2H_2O$), thioacetamide (C_2H_5NS), acetic acid and ethanol. All of the chemicals were purchased from Shanhai Chemical Reagent Company in analytical grade, and were used without further purification

2.2 Synthesis of $SrZrO_3$ photocatalyst

$SrZrO_3$ photocatalyst were synthesized by hydrothermal method according to the previous literature[30]. Typically, 1.164 g $Sr(NO_3)_2$ and 1.608 g $ZrOCl_2·8H_2O$ were dissolved in 60 mL 12 mol/L KOH solution and stirred 1 h at ambient temperature by using a magnetic stirrer. Then the mixture was transferred to a 100 mL Teflon-lined stainless steel autoclave, heated up to 200°C and kept for 24 h. After cooling naturally, the product was centrifuged and washed with distilled water, diluted acetic acid to remove some $SrCO_3$ by-products, and ethanol several times. After that, the sample was vacuum dried at 60 °C for 6 h. It is worth noting that the KOH solution was pre-prepared or the temperature would rise up to over 100 °C resulting in the inhomogeneous formation of $SrZrO_3$ crystal.

2.3 Synthesis of MoS_2 crystal

The MoS_2 crystal was synthesized by hydrothermal method. Typically, 0.807 g $Na_2MoO_4·2H_2O$ and 1.2522 g C_2H_5NS was dissolved in a 100 mL beaker containing 20 mL distilled water and 20 mL ethanol, and the mixture was stirred 30 min under a magnetic stirrer. Then the solution was transferred in a 100 mL Teflon-lined stainless-steel autoclave, sealed and heated to 200 °C for 48 h. After cooling naturally, the product was centrifuged, washed with distilled water and ethanol several times. The sample was vaccum dried at 60 °C for 6 h.

2.4 Synthesis of $MoS_2/SrZrO_3$ heterocatalyst

The formation process of $MoS_2/SrZrO_3$ heterocatalyst was described as follows. 0.5g as-prepared $SrZrO_3$ was dissolved in the mixture containing 20 mL distilled water and 20 mL ethanol, a certain quality $Na_2MoO_4·2H_2O$ and C_2H_5NS was then added into the solution and the molar ration of $Na_2MoO_4·2H_2O$ and a certain quality $Na_2MoO_4·2H_2O$ and C_2H_5NS was then added into the solution and the molar ration of $Na_2MoO_4·2H_2O$ and C_2H_5NS was 1 : 5. The obtained suspension was sonicated for 10 min and stirred 30 min in order to disperse uniformly. The solution was sealed in a 100 mL Teflon-lined stainless-steel autoclave and heated in an electric oven at 200 °C for 48 h. After cooling to the room temperature, the product was separated by centrifugation, washed with distilled water and ethanol several times. Finally, the catalysts were dried in vacuum at 60 °C for 6 h. The prepared samples with 0.01, 0.05, 0.1, 0.2, 0.5, 1, 2, 5, 7, 10 wt % MoS_2, defined as the weight ration of MoS_2 to $SrZrO_3$, were named as SM1, SM2, SM3, SM4, SM5, SM6, SM7, SM8, SM9, SM10.

2.5 Characterization of photocatalyst

X-ray diffraction (XRD) patterns were recorded on Bruker D8-Discover with Cu Kα radiation (λ=1.54178Å). The transmission electron microscopy (TEM, Hitachi H-600) and the scanning electron microscopy (SEM, FEI Inspect F50) were used to characterize the morphologies and size of the synthesized product. UV-vis absorption spectra were measured on a Shimadzu UV-3100 spectrometer. The chemical composition analysis of the sample surfaces was characterized by X-ray photoelectron spectra (XPS) (VG Multiab-2000) using a PHI Quantum 2000 XPS system with a monochromatic Al Kα source and charge neutralizer. All of the spectra were calibrated to C 1s peak at 284.6 eV.

2.6 Photocatalytic activity test

Photocatalytic reactions of hydrogen evolution were carried out in a 250 mL Pyrex flask at room temperature and atmospheric pressure, and 100 W mercury lamp (365nm, Shanghai Special Lighting Factory) was used as the light source. Typically, photocatalyst (0.2 g) was dissolved in 250 mL aqueous solution containing Na_2S (0.35M) and Na_2SO_3 (0.25M) as electron donors. Prior to irradiation, the suspension was sonicated for 20 min and bubbled with N_2 for 30 min to remove the dissolved oxygen. Then the photocatalyst was irradiated with ultraviolet light from the Hg lamp. The amount of H_2 was determined by gas chromatograph (GC-14C, Shimadzu, Japan, TCD, nitrogen as a carrier gas and 5 Å molecular sieve column).

3. Results and discussion

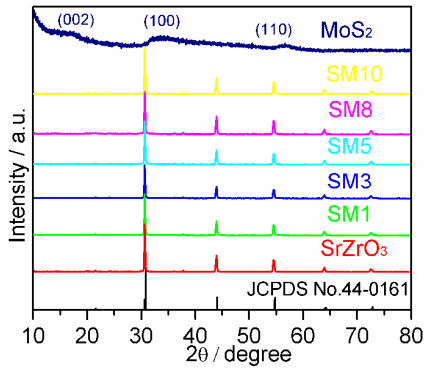

Fig. 1 XRD patterns of $SrZrO_3$, SM1，SM3，SM5，SM8, SM10, MoS_2 and standard pattern of $SrZrO_3$

In order to investigate the changes of phase structures and crystal form of the as-prepared samples, X-ray diffraction measurement was performed. Fig.1 shows the XRD patterns of $SrZrO_3$, MoS_2 and $MoS_2/SrZrO_3$ synthesized by hydrothermal method. All the peaks were assigned as orthorhombic perovskite $SrZrO_3$ structure (JCPDS card 44-0161) with cell parameter a=5.819 Å, b=8.204 Å and c=5.797 Å in Pnma (62) space group, and several typical peaks at 2θ=21.6°，24.2°, 30.7°，36.2°， 37.9°，44.1°，45.5°, 54.7°，64.0°, 72.7° were observed and corresponding to（020）,（111）,（200）,（211）,（220）,（202）,（212）,（240）,

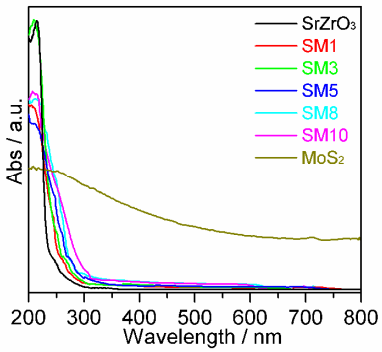

Fig.2 UV-vis absorption spectra of SrZrO3, SM1, SM3, SM5, SM8, SM10 and MoS_2 samples

（400）and（402）planes, respectively. For pure MoS_2 crystal, peaks are ascribed to (002), (100) and (110) planes with hexagonal phase MoS_2 (JCPDS card 37-1492)[27, 31]. However, no obvious peaks of heterojunctions attributed to MoS_2 phase were observed in the $MoS_2/SrZrO_3$ samples mainly due to its low loading content, high distribution of the MoS_2 component and weak crystallization in these catalysts[32-34].

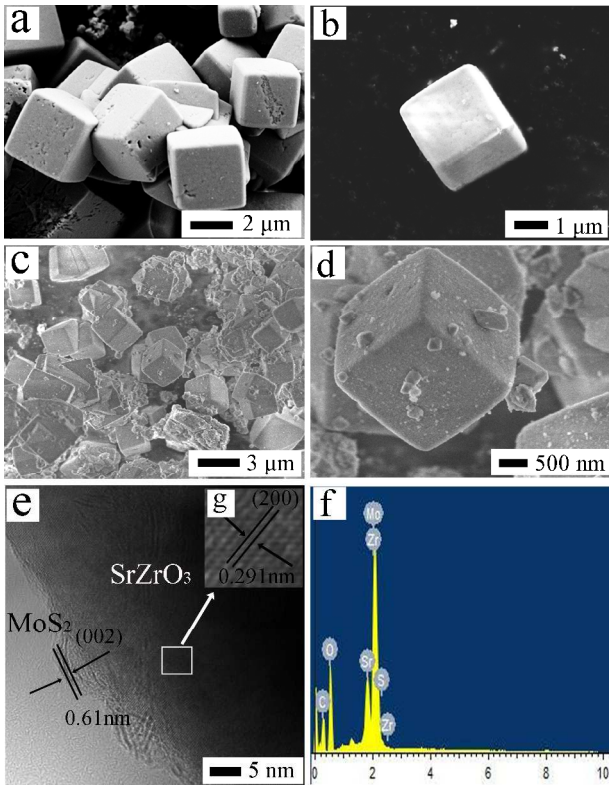

Fig.3 (a) SEM images of $SrZrO_3$, (b)SEM images of MoS_2, (c-d) SEM images of SM8, (e,g) HRTEM images of SM8, (f) EDX pattern of SM8 photocatalyst in (c)

Fig.2 demonstrated the UV-vis absorption specra of pure $SrZrO_3$ and $MoS_2/SrZrO_3$ heterostructures. For pure $SrZrO_3$ sample, the absorption at 230 nm was supposed to the instinct band gap absorption, and the band gap of $SrZrO_3$ is 5.4 eV which is close to 5.6 eV that literature reported[18, 35, 36]. And the absorption of MoS_2 was blue-shifted relative to the bulk MoS_2 having a band edge at 1040 nm[27, 37]. Noticeably, a similar UV-vis absorption curves were observed, and the absorption edges of heterojunction is red-shifted gradually when the increasing amount of MoS_2 crystal was loaded on the surface of $SrZrO_3$. Further, the absorption band of $MoS_2/SrZrO_3$ was located at the UV region, indicating an excellent UV absorption at this area.

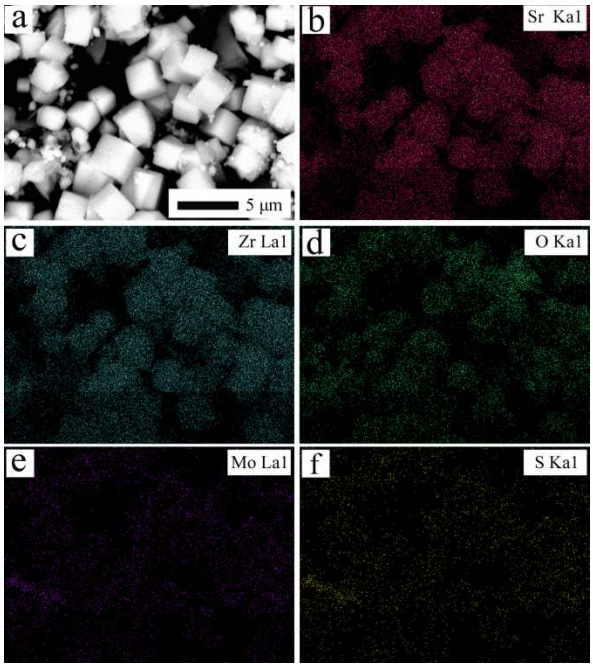

Fig.4 (a) SEM image of SM8, and (b-f) the corresponding EDX mapping of $MoS_2/SrZrO_3$ at the region shown in (a), indicating spatial distribution of Sr, Zr, O, Mo, S, respectively.

The morphologies of as-prepared catalysts were characterized by scanning electron microscope (SEM) and transmission electron microscope (TEM) , which was shown in Fig.3. The morphology of $SrZrO_3$ (Fig.3a) shows a cubic structure with an average side length of 2 μm，and the sizes and shapes of pure $SrZrO_3$ and SM8 remained almost the same after loading MoS_2, which is demonstrated by the comparison of Fig. 3c with Fig. 3a. For pure MoS_2 (Fig.3b), the successfully synthesized MoS_2 was layer-structured, which is flower-like nanostructure with average diameter of 200 nm. Furthermore, the MoS_2 small nanoflakes loading on the surface of $SrZrO_3$ were observed from Fig.3d. The elemental composition of the photocatalyst was examined by energy dispersive X-Ray spectroscopy (EDX) ananlysis, Fig.3f. The presence of Sr, Zr, O, Mo and S elements were confirmed by EDX. The HRTEM image of $MoS_2/SrZrO_3$ in Fig.3e indicats the lattice spacing with an interplanar distance of 0.291 nm and 0.61 nm, which are corresponding to the (200) and (002) d–spacing of the orthorhombic phase of $SrZrO_3$ and hexagonal MoS_2 [5, 27, 38], respectively. Herein, the HRTEM image is just an indirect proof demonstrating the existence of MoS_2 in $MoS_2/SrZrO_3$ heterojunctions.

To confirm the formation of $MoS_2/SrZrO_3$ heterojunction, the SEM and TEM analysis of $SrZrO_3$ have been characterized before and after loading MoS_2. In addition to this, SEM-EDX mapping has also been detected to show the elemental distribution of Sr, Zr, O, Mo and S, which was presented in Fig.4,

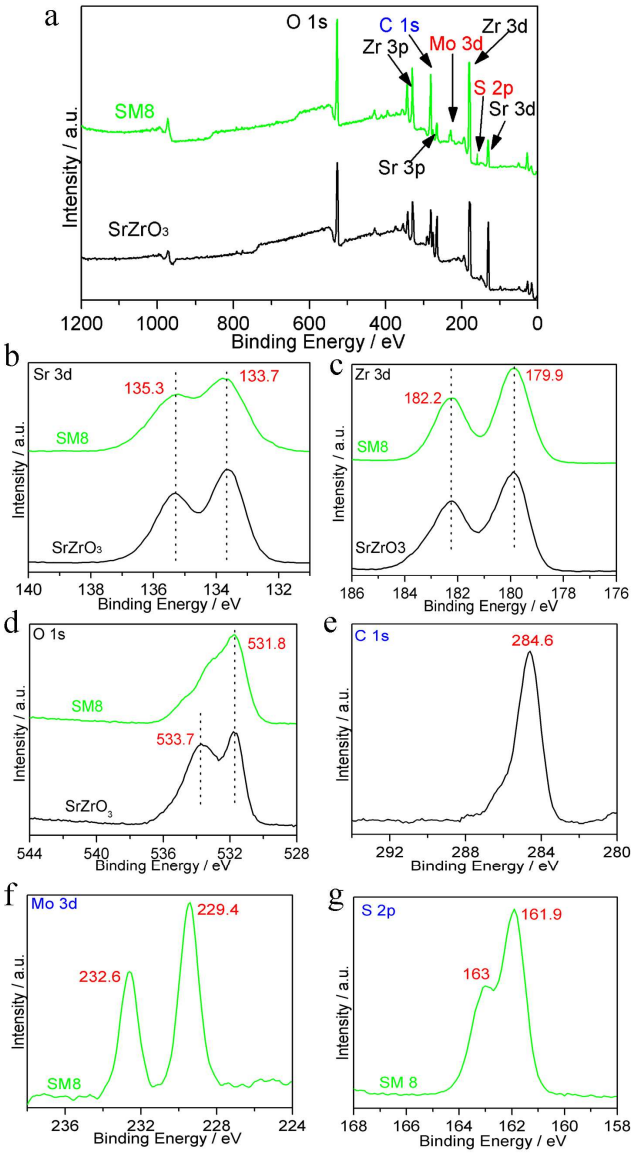

Fig.5 (a) XPS survey spectra of sample $SrZrO_3$ and SM8, (b-f) High resolution XPS spectra of Sr, Zr, O, Mo and S.

and the selected area of EDX-mapping analysis was shown in Fig.4a. Obviously, homogeneous distributions of Sr, Zr and O were observed in the particle (Fig.4b-d) which is consistent to the SEM image. The distribution of elements of Mo and S were also displayed uniformly with low density (Fig.4e-f).

To further investigated the chemical composition and elemental status of $SrZrO_3$ and $MoS_2/SrZrO_3$, XPS analysis was carried out and presented in Fig.5. The content of MoS_2 lower than 0.1 % cannot be detected by XPS, and the different of all heterojunctions is the smoothness with different MoS_2 content, thus, we chose SM8 to investigate the XPS of the elements. The XPS peak for C 1s at 284.6 eV is due to adventitious carbon from the XPS instrument. Fig.5a gives the comparision of XPS spectra of $SrZrO_3$ and SM8 samples. The compositions of high resolution XPS of Sr, Zr and O elements for $SrZrO_3$ and SM8 were shown in Fig.5b-d. No apparent differences except O were observed when MoS_2 loading on the surface of $SrZrO_3$, indicating the introduced MoS_2 has little influence on the chemical valence[33]. Two peaks of Sr 3d in Fig.4b at 135.3 and 133.7 eV are assigned to Sr 3d3/2 and Sr 3d5/2, and the binding energies corresponding to Zr 3d3/2 and Zr 3d5/2 are 182.2 and 179.9 eV, respectively[32]. The binding energy difference of O 1s was 533.7 eV due to the absorbed oxygen in $SrZrO_3$ sample[34], and the binding energy located at 531.8 eV is assigned to O 1s. The peaks of Mo 3d (Fig.5e) at 232.6 and 229.4 eV are attributed to Mo(+4) 3d3/2 and Mo(+4) 3d5/2, respectively[22]. It can be clearly seen from Fig.5f that the measured binding energies of S 2p1/2 and S 2p3/2 are corresponding to 163 and 161.9 eV, respectively[22, 27, 39]. The atomic percentage of Mo and S analyzed by XPS was 3.876:7.481, which is close to 1:2.Taken all, the existence of MoS_2 and $SrZrO_3$ in SM8 sample was further confirmed by high resolution of XPS spectra, which is consistent of XRD and TEM analysis.

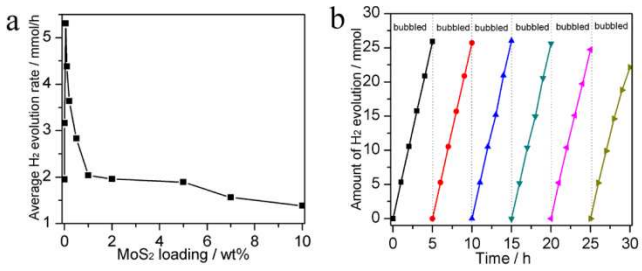

Fig.6 (a) Photocatalytic activity of $MoS_2/SrZrO_3$ catalysts with loading different amount of MoS_2, and (b) Time course of H_2 evolution over 0.05 MoS_2(0.05 wt %)/ $SrZrO_3$ photocatalyst.

In order to investigated the photocatalytic performance of $SrZrO_3$ photocatalyst before and after loading MoS_2, a serious of experiments have been carried out and the results have been shown in Fig.6a. It is clear that the rate of H_2 evolution was obviously enhanced when loading a relative small amount of MoS_2 with 0.05 wt%. The rate of H_2 evolution for pure $SrZrO_3$ phocatalyst was 1.95 mmol/h, while the rate of H_2 evolution of $MoS_2/SrZrO_3$ was 5.31 mmol/h, nearly 2.7 times of pure samples, which is due to the effect of heterojunction between MoS_2 and $SrZrO_3$. As can be seen, H_2 production was gradually decreased or even lower than pure $SrZrO_3$ as the increasing amount of MoS_2. It is mainly due to several reasons: the decrease of $SrZrO_3$ surface active sites resulting from the excessive loading MoS_2 cluster; deterioration of catalytic properties of $SrZrO_3$ cluster; decrease of irradiation passing through the sacrifice solution[40]. The stability and recycling performance of photocatalysts are important factors in the commercial applications, thus, time course of H_2 production over $MoS_2/SrZrO_3$ was performed (Fig.6b). Clearly, the average rate of H_2 evolution was nearly unchanged after 30 h reaction, indicating an excellent stability of photocatalyst.

A possible mechanism of photocatalytic H_2 evolution over $MoS_2/SrZrO_3$ heterojunction was proposed and depicted in Fig.7. The $SrZrO_3$ photocatalyst absorbed enough energy greater than band gap under UV light irradiation, and generated electron was easily transferred to conduction band, leaving photo-generated holes in the valence band. The catalytic activities without MoS_2 loading were lower because of the recombination between photo-generated electrons and holes. While, the H_2 evolution was

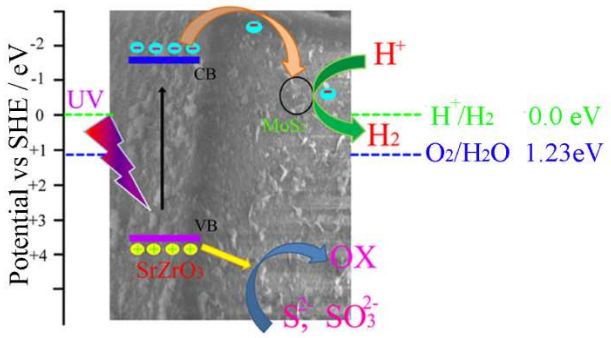

Fig.7 Mechanism of photocatalytic water splitting over $MoS_2/SrZrO_3$ photocatalysts under UV light.

significantly enhanced after loading MoS_2 because of the rapid transfer of the photo-generated electrons from the conduction band of $SrZrO_3$ samples to MoS_2 which is due to the higher conduction band of $SrZrO_3$ than that of MoS_2. At the same time, the H^+ was reduced to H_2 with the MoS_2 trapping of photo-generated electrons, and whereas holes of $SrZrO_3$ crystals in the valence band oxidize S^{2-} and SO_3^{2-}on the surface of $SrZrO_3$. The heterojunctions between $SrZrO_3$ and MoS_2 was considered as an important factor for the remarkably improved H_2 evolution.

4. Conclusions

In summary, the $MoS_2/SrZrO_3$ heterojunction was synthesized for the first time through two-step hydrothermal reaction. The highest of H_2 evolution rate of 5.31 mmol/h was obtained with 0.05 wt % MoS_2 loading on the surface of $SrZrO_3$ under UV irradiation, and the mechanism of process of H_2 evolution was also proposed. Furthermore, the amount of MoS_2 plays an important in photocatalytic activities, which were might due to the changes of active sites, band gaps and irradiation opacity. Obviously, the influences of MoS_2 in $MoS_2/SrZrO_3$ heterogenerous photocatalyst were matching the band energy and suppressing the recombination between photogenerated electron and holes, resulting in the enhancement of H_2 evolution.

Acknowledgement

This work was financially supported by the National Nature Scie nce Foundation of China (No. 31070517) and the National Basic Research Program of China (973 Program, No. 2013CB932902).

Notes and references

School of Chemistry and Chemical Engineering, Southeast University, Nanjing, 211189, P.R. China.
Fax: +86 02552090620; Tel: +86 025 52090621; E-mail: jczhou@seu.edu.cn (Prof. J. Zhou)
† These authors contributed equally to this work.

1 Y. Q. Zhong, K. Ueno, Y. Mori, X. Shi, T. Oshikiri, K. Murakoshi, H. Inoue and H. Misawa, *Angew. Chem. Int. Ed.*, 2014, **53**, 1.
2 Z. J. Han, F. Qiu, R. Eisenberg, P. L. Holland and T. D. Krauss, *Science*, 2012, **338**, 1321.
3 H. Kisch, *Angew. Chem. Int. Ed.*, 2013, **52**, 812.
4 A. Kudo and Y. Miseki, *Chem. Soc. Rev.*, 2009, **38**, 253 .
5 X. Zong, H. J. Yan, G. P. Wu, G. J. Ma, F. Y. Wen, L Wang and C. Li, *J. Am. Chem. Soc.*, 2008, **130**, 7176.
6 T. F. Jaramillo, K. P. Jorgensen, J. Bonde, J. H. Nielsen, S. Horch and I. Chorkendorff, *Science*, 2007, **317**, 100.
7 A. Fujishima and K. Honda, *Nature*, 1972, **238**, 37.
8 H. I. Karunadasa, C. J. Chang and J. R. Long, *Nature*, 2010, **464**, 1329.
9 F. Bai, Z. C. Sun, H. M. Wu, R. E. Haddad, X. Y. Xiao,and H. Y. Fan, *Nano Lett.*, 2011, **11**, 3759.
10 Y Zhong, Z. X. Wang, R. F. Zhang, F. Bai, H. M. Wu, R. Haddad, and H. Y. Fan, *ACS Nano*, 2014, **8**, 827.
11 F. Bai, Z. C. Sun, H. M. Wu, R. E. Haddad, E. N. Coker, J. Y. Huang,M. A. Rodriguez, and H. Y. Fan, *Nano Lett.*, 2011, **11**, 5196.
12 J. C. Colmenares and R. Luque, *Chem. Soc. Rev.*, 2014, **43**, 765.
13 Y. Q. Qu and X. F. Duan, *Chem. Soc. Rev.*, 2013, **42**, 2568.
14 Y. Miseki, H. Kato and A. Kudo, *Energy Environ. Sci*., 2009, **2**, 306.
15 Y. J Su, K. L. Pan and M. B. Chang, *Int. J. Hydrogen. Energ.*, 2014, **39**, 4917.
16 L. Q. Jing, Y. C. Qu, H. J. Su, C. H. Yao and H. G. Fu, *J. Phys. Chem. C*, 2011, **115**, 12375.
17 E. A. Slonimskaya and A. V. Belyakov, *Glass Ceram.*, 2001, **58**, 1.
18 A. Y. Zhang, M. K. Lü, S. F. Wang, G. J. Zhou, S. M. Wang and Y. Y. Zhou, *J. Alloy. Compd.*, 2007, **433**, 7.
19 I. R. Shein, V. L. Kozhevnikov and A. L. Ivanovskii, *Solid State Sci.*, 2008, **10**, 217.
20 M. Daturi and G. Busca, *Chem. Mater.*, 1995, **7**, 2115
21 Y. L. Tian, B. B. Chang, Z.C. Yang, B. C. Zhou, F. N. Xi and X. P. Dong, *RSC Adv.*, 2014, **4**, 4187.
22 Y. Liu, Y. X. Yu and W. D. Zhang, *J. Phys. Chem. C*, 2013, **117**, 12949.
23 J. L. Li, X. J. Liu, L. K. Pan, W. Qin, T. Q. Chen and Z. Sun, *RSC Adv*., 2014, **4**, 9647.
24 H. I. Karunadasa, E. Montalvo, Y. Sun, M. Majda, J. R. Long and C. J. Chang, *Science*, 2012, **335**, 698.
25 Y. G. Li, H. L. Wang, L. M. Xie, Y. Y. Liang, G. S. Hong and H. J. Dai, *J. Am. Chem. Soc.*, 2011, **133**, 7296.
26 F. Meng, J. T. Li, S. K. Cushing, M. J. Zhi and N. Q. Wu, *J. Am. Chem. Soc.*, 2013, **135**, 10286.
27 W. J Zhou, Z. Y. Yin, Y. P. Du, X. Huang, Z. Y. Zeng, Z. X. Fan, H. Liu, J. Y. Wang and H. Zhang, *Small*, 2013, **9**, 140.
28 G. Zhou, X. Y. Xu, J. Y. Yu, B. Feng, Y. Zhang, J. G. Hu and Y. X. Zhou, *CrystEngComm*, 2014, DOI:10.1039/c4ce01169d.
29 X. Zong, G. P. Wu, H. J. Yan, G. J. Ma, J. Y. Shi, F. Y. Wen, L. Wang and C. Li, *J. Phys. Chem. C*, 2010, **114**, 1963.
30 T. N. Ye, Z. H. Dong, Y. N. Zhao, J. G. Yu, F. Q. Wang, S. K. Guo and Y. C. Zou, *CrystEngComm*, 2011, **13**, 3842.
31 Y. T. Lu, D. D. Wang, P. Yang, Y. K. Du and C. Lu, *Catal. Sci. Technol.*, 2014, **4**, 2650.
32 J. R. Ran, J. G. Yu and M. Jaroniec, *Green. Chem.*, 2011, **13**, 2708.
33 L. F. Qi, J. G. Yu and M. Jaroniec, *Phys. Chem. Chem. Phys.*, 2011, **13**, 8915.
34 Y. Lee, J. Lee, T. Noh, D. Byun, K. Yoo, K. Yamaura and E. Takayama-Muromachi, *Phy.s Rev. B*, 2003, **67**, 113101.
35 R. Schafranek, J. D. Baniecki, M. Ishii, Y. Kotaka, K. Yamanka and K. Kurihara, *J. Phys. D: Appl. Phys.*, 2012, **45**, 55303.
36 N. X. Li, B. Y. Zhou, P. H. Guo, J. C. Zhou and D. W. Jing, *Int. J. Hydrogen Energ.*, 2013, **38**, 11268.
37 U. Oemar, P.S. Ang, K. Hidajat and S. Kawi, *Int. J. Hydrogen Energ.*, 2013, **38**, 5525.
38 J. H. Liu, L. Zhang, Q. W. Tian, N. X. Li, J. C. Zhou and Y. M. Sun, *J. Mater. Chem. A*, 2014, DOI: 10.1039/C4TA04984E
39 V. O. Koroteev, L. G. Bulusheva, I. P. Asanov, E. V. Shlyakhova, D. V. Vyalikh and A. V. Okotrub, *J. Phys. Chem. C*, 2011, **115**, 21199.
40 J. G. Yu, Y. Hai and B. Cheng, *J. Phys. Chem. C*, 2011, **115**, 4953.